Research Article | Vol. 31, No. 8 / 10 Apr 2023 / Optics Express 13357
Optics EXPRESS

Dynamically switchable self-focused thermal emission

ROMIL AUDHKHASI,[1] YURUI QU,[2] MING ZHOU,[3] ZONGFU YU,[2] AND MICHELLE L. POVINELLI[1,*]

[1]*Ming Hsieh Department of Electrical and Computer Engineering, University of Southern California, Los Angeles, California 90089, USA*
[2]*Department of Electrical and Computer Engineering, University of Wisconsin-Madison, Madison, Wisconsin 53706, USA*
[3]*Department of Electrical Engineering, Stanford University, Stanford, California 94305, USA*
[*]*povinell@usc.edu*

Abstract: The ability to manipulate thermal emission is paramount to the advancement of a wide variety of fields such as thermal management, sensing and thermophotovoltaics. In this work, we propose a microphotonic lens for achieving temperature-switchable self-focused thermal emission. By utilizing the coupling between isotropic localized resonators and the phase change properties of VO_2, we design a lens that selectively emits focused radiation at a wavelength of 4 µm when operated above the phase transition temperature of VO_2. Through direct calculation of thermal emission, we show that our lens produces a clear focal spot at the designed focal length above the phase transition of VO_2 while emitting a maximum relative focal plane intensity that is 330 times lower below it. Such microphotonic devices capable of producing temperature-dependent focused thermal emission could benefit several applications such as thermal management and thermophotovoltaics while paving the way for next-generation contact-free sensing and on-chip infrared communication.

1. Introduction

Several applications such as thermal management and sensing require precise control over the spectral selectivity and directionality of thermal emission. Historically, thermal emission had been considered incoherent. In 2002, Greffet et al. showed that coherent wave effects can be exploited in periodically-patterned SiC films to achieve directional thermal emission in the long-wave infrared (IR) [1]. Since then, several microphotonic devices have been proposed and investigated for generating tailored spectral [2–4] or directional [5–9] emission profiles in the infrared.

In recent years, there has been growing interest in achieving more exotic functionalities such as the generation of focused thermal emission. It is important to note that devices capable of generating focused thermal emission are fundamentally different from conventional metalenses. A conventional lens uses an array of scatterers to impart a phase profile to an incident monochromatic plane wave to focus it at a desired location in space [10]. On the other hand, a thermal lens is designed to focus emission from multiple, incoherent thermal sources that reside within it.

Recent work from Chalabi et al. showed that an array of SiC beams on a SiC film can be used for achieving self-focused thermal emission [11]. The working principle of this device was based on the existence of surface phonon polariton modes in SiC in the long-wave IR. Consequently, the wavelength range of operation of the lens was limited to a narrow spectral band. More recently, Zhou et al. numerically demonstrated self-focused thermal emission in a freely-suspended array of coupled, dielectric nanorods [12]. The nanorods were considered to be dispersionless with only the central nanorod having a non-zero material loss. The sizes of the nanorods and the spacing between them could be adjusted to tune the operating wavelength of the lens.

#484555 https://doi.org/10.1364/OE.484555
Journal © 2023 Received 28 Dec 2022; revised 10 Mar 2023; accepted 22 Mar 2023; published 7 Apr 2023

Optics EXPRESS

In this work, we adopt the modeling approach used by Zhou et al. to design a practically realizable lens with temperature-dependent, self-focused thermal emission. The lens relies upon the phase change properties of vanadium oxide (VO_2) that behaves as an insulator below a temperature of 340 K and a metal above it. This phase transition is accompanied by a dramatic change in optical properties. Previous studies have widely investigated VO_2-based microstructures for temperature-tunable thermal emission [13–21]. Through direct calculation of thermal emission, we show that our lens focuses intensely above the phase transition of VO_2 while emitting a relative focal plane intensity that is 330 times lower below it.

We envision the utility of our switchable thermal lens in a wide variety of applications ranging from thermal management and thermophotovoltaics to contact-free sensing and on-chip optical communication.

2. Methods

In the following subsection, we discuss the design of our temperature-switchable lens along with the working principle of its constituent resonators. Details of the lens optimization procedure are provided in the subsequent subsection.

2.1. Switchable thermal lens design

Figure 1(a) shows a schematic of our switchable thermal lens. It consists of 25 silicon nanorods on a 0.1 μm thick Al_2O_3 layer. The central nanorod has a VO_2 cap on the top. For simplicity, we only consider the behavior of our structure at 300 and 350 K, hereby referred to as the cold and hot states, respectively. The lens is optimized to focus at a wavelength of 4 μm in the hot state. We consider the lens to be infinite along the y direction and as having a width of 80 μm along the x direction.

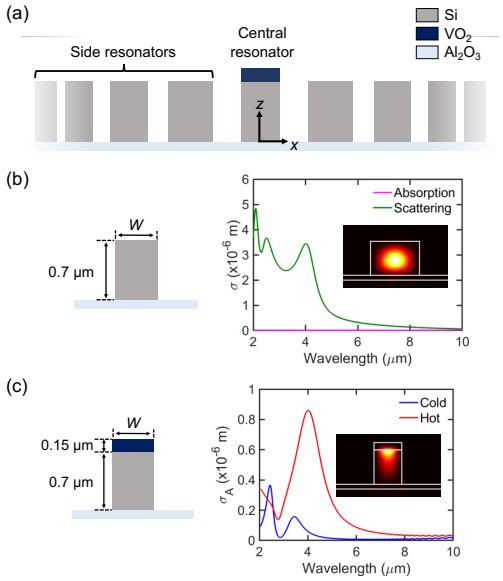

Fig. 1. (a) Schematic of our switchable thermal lens. (b) (left panel) Side resonator with $W = 0.95$ μm. (right panel) Absorption and scattering cross sections of the side resonator. Inset shows $|H|^2$ for the side resonator at $\lambda = 4$ μm. (c) (left panel) Central resonator with $W = 0.54$ μm. (right panel) Absorption cross sections for the cold and hot states of the central resonator. Inset shows $|H|^2$ for the hot state of the central resonator at $\lambda = 4$ μm.

Optics EXPRESS

The side resonators of our lens are chosen to be 0.7 μm tall Si nanorods with width W (left panel of Fig. 1(b)). The right panel of Fig. 1(b) shows the absorption and scattering cross sections for a nanorod with $W = 0.95$ μm. This value of W is chosen to get a magnetic dipole Mie resonance at a wavelength of 4 μm. The cross sections are calculated by simulating the resonators in Lumerical FDTD with a broadband Total Field Scattered Field (TFSF) source. Each simulation consists of a 2D domain with PML boundary conditions on all four sides. The optical constants of Si and Al_2O_3 are taken from the built-in material library while those of VO_2 are taken from Ref. [22]. The absorption and scattering cross sections are recorded using a 2D box of power flux monitors inside the total field and scattered field regions, respectively.

One can observe that the scattering cross section is orders of magnitude larger than the absorption cross section, implying that the resonators are effectively lossless. The squared magnitude of the magnetic field on resonance, $|H|^2$, shown in the inset resembles that of a magnetic dipole Mie resonance. Such resonances in freely suspended dielectric nanorods have been shown to exhibit isotropic far-field radiation profiles [12]. In our thermal lens, we mount the resonators on a 0.1 μm thick free-standing Al_2O_3 membrane to ensure nearly isotropic emission. Thin Al_2O_3 layers on back-etched Si wafers have previously been used as optically transparent membranes for the fabrication of metasurfaces in the infrared [23].

Similar to the original design approach proposed by Zhou et al., we choose a central resonator that is sufficiently lossier than the side resonators. To accomplish this, we incorporate a 0.15 μm thick VO_2 cap on the top of the central resonator (left panel of Fig. 1(c)). The right panel of Fig. 1(c) shows the absorption cross sections of the central resonator for $W = 0.54$ μm in the cold and hot states. One can observe that the absorption cross section has a peak at 4 μm in the hot state which blue shifts and reduces in height in the cold state. This change can be understood by looking at the squared magnitude of the magnetic field in the hot state shown in the inset. The field is mostly concentrated at the interface between Si and VO_2 and has sufficient overlap with the VO_2 cap. As a result of this field overlap, the resonance wavelength and absorption cross section are sensitive to changes in the optical properties of VO_2. As VO_2 in the hot state is lossier and has higher refractive index than the cold state, an increase in temperature causes a significant change in the absorption cross section.

2.2. Lens optimization

The widths and center-to-center separations of the nanorods are determined from a gradient descent optimization based on temporal coupled-mode theory (CMT) [12]. We regard our thermal lens as an array of coupled resonators. This allows us to write the emitted field intensity in terms of the individual resonator properties and inter-resonator coupling. As the resonators in our structure support Mie-like magnetic dipole resonances, we consider them as 2D isotropic emitters. In this case, the near-field coupling between any pair of resonators can be written in terms of their radiative decay rates and relative positions [24]. We calculate the individual properties of the resonators such as their resonance frequencies and decay rates from their absorption and scattering cross sections [25]. The individual resonator parameters and the inter-resonator coupling constants as a function of W together form a catalog of CMT parameters.

We define our objective function as the squared norm of the difference between the intensity emitted by the structure at the designed focal plane and the target intensity profile. The structure is characterized by a parameter set that includes the resonant frequencies and positions of all the resonators. This parameter set is optimized using a gradient descent process. At each step of the optimization process, the CMT catalog is used along with the adjoint method to compute the gradient of the objective function. While the current work discusses the design of a lens in which the central resonator is lossier than the side resonators, the adjoint optimization method can in principle be used to design a lens in which all resonators have comparable loss.

Optics EXPRESS

Figure 2 presents the widths of the nanorods, W as a function of the position of their centers, x. The origin of the x-axis is assumed to be located at the center of the central resonator. One can observe that the nanorod width profile is symmetrical about the origin. This ensures that the field intensity emitted by the lens is symmetrical about the y-z plane passing through its center. The average center-to-center separation between the nanorods is 3.2 µm while the widths of the nanorods vary between 0.26 µm and 0.88 µm.

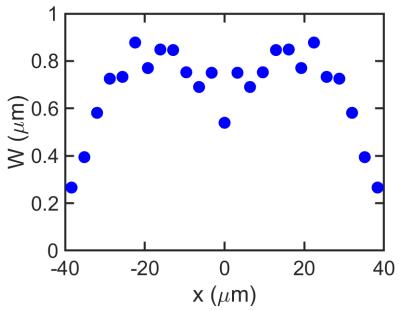

Fig. 2. Variation of nanorod widths for the optimized lens with the position of their centers.

3. Results

In this section, we calculate the far-field thermal emission from the optimized lens in both temperature states. Such a calculation must consider incoherent emission from a large number of thermal sources distributed across the structure. In the following subsections, we discuss our method for direct calculation of thermal emission from such mixed-material structures and provide an illustration of the temperature-dependent focusing effect.

3.1. Direct calculation of thermal emission in mixed-material systems

To emulate thermal emission, we perform multiple simulations using Lumerical FDTD, each with a single, randomly oriented magnetic dipole placed at a random location inside the lens (Fig. 3(a)). The dipole location in each of the simulations is chosen so as to have an overall unform distribution of dipoles in the lens. The number of dipoles in different parts of the lens is directly proportional to their respective areas. Each simulation consists of a 2D domain with PML boundary conditions on all four sides. We note that simulating the entire x-z space up to the focal spot can result in large memory consumption. To mitigate this, near-field data is recorded using a frequency domain power monitor and projected to different points on the x-z plane.

The far-field intensities obtained from each of these simulations are multiplied by a weighting factor and added together (Fig. 3(b)). Similar approaches have been used for calculating thermal emission in mixed-material systems [26,27]. The weighting factor for a dipole in the ith simulation located in a material A is given as:

$$w_i = \mathrm{Im}(\varepsilon_A)\frac{\hbar\omega^3}{\exp\left(\frac{\hbar\omega}{k_B T}\right) - 1} \tag{1}$$

Here $Im(\varepsilon_A)$ denotes the imaginary part of the permittivity of material A, ω is the operating frequency, T is the temperature, $\hbar$ is the modified Planck's constant and k_B is the Boltzmann constant. The weighting factor in Eqn. (1) considers the contribution of material loss (represented by $\mathrm{Im}(\varepsilon_A)$) and the blackbody radiation intensity to thermal emission. Due to the symmetry of the lens structure, the resultant field intensity must be symmetrical about the y-z plane passing

Optics EXPRESS

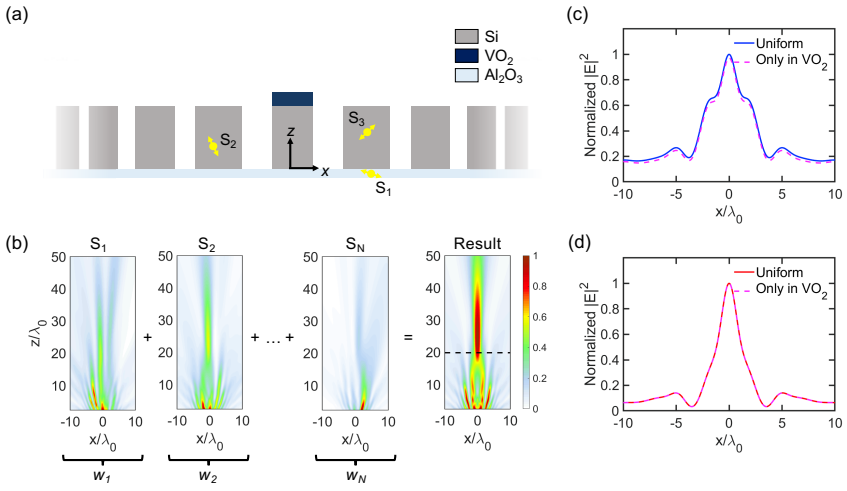

Fig. 3. (a) Schematic describing the dipole distribution for a thermal emission calculation using N simulations. Here, we only show simulations S_1, S_2 and S_N for clarity. (b) The resultant field intensity is calculated by adding the field intensities from individual dipole simulations multiplied by their respective weighting factors. The resultant field intensity shown in the figure is calculated using $N = 300$ and normalized to its own maximum. Focal plane field intensities for the lens in the cold and hot states are shown in (c) and (d), respectively. The solid lines are the intensities obtained by taking all dipoles into account while the dashed lines are the contributions of only dipoles placed in the VO_2 cap.

through its center. To ensure this, we also add mirror-flipped field intensities corresponding to all the dipoles to the overall sum.

We run a calculation with 300 dipoles and present the field intensities at the focal plane ($20\lambda_0$) for the cold and hot states in Figs. 3(c) and (d), respectively. As the VO_2 cap occupies about 0.4% of the total area of the lens, only one out of the 300 simulations has a dipole inside it. The solid lines in Figs. 3(c) and (d) show the field intensities obtained by adding emission from all dipoles in the structure while the dashed lines show the result only for the dipole placed in the VO_2 cap. One can observe that in both temperature states, the field intensity from the dipole in the VO_2 cap is approximately equal to that obtained by taking all the dipoles in the structure into account. Additionally, the difference between the two field intensities is much less noticeable in the hot state as compared to the cold state.

These results can be understood by an approximate numerical argument. At a wavelength of 4 μm, the imaginary part of the permittivity for VO_2 in the cold state is 1.38. On the other hand, Im(ε) for Si and Al_2O_3 are 2.9×10^{-5} and 2×10^{-3}, respectively. The total areas occupied by VO_2, Si and Al_2O_3 are 0.08, 11.9 and 8 μm^2 respectively. We consider the product of the area occupied by a given material and the imaginary part of its permittivity as an estimate of its contribution to the overall emission. These values for VO_2 in the cold state, Si and Al_2O_3 are 0.11, 3×10^{-4} and 0.016 μm^2, respectively. In the hot state, VO_2 has an imaginary part of permittivity equal to 58.9 and hence, the value of the product is 4.7 μm^2. In both temperature states, the area-permittivity product for VO_2 is significantly greater than that for Si and Al_2O_3. Therefore, it is reasonable to assume that the overall emission from the lens comes primarily from VO_2. This assumption is consistent with our observation in Figs. 3(c) and (d).

To get results that are statistically significant, we must have a sufficiently large number of dipoles in the VO_2 cap. As mentioned previously, the VO_2 cap occupies only about 0.4% of the total lens area. Therefore, a calculation with N dipoles in the VO_2 cap will require a total of $250N$

Optics EXPRESS

dipoles distributed uniformly across the structure. Such a calculation would incur an unnecessary computational cost as most of these dipoles will not contribute to the overall emission from the lens. To avoid this computational expense, we perform all our calculations from here onwards with dipoles placed only in the VO_2 cap.

3.2. Temperature-switchable thermal focusing

Figure 4(a) shows a schematic of the lens in which all dipoles are placed only in the VO_2 cap. We vary the number of dipoles till the obtained spatial field intensity profiles have converged. Figure 4(b) presents the resulting field intensities in the x-z plane at a wavelength of 4 µm for a calculation with 600 dipoles. The field intensities in both temperature states are normalized to the maximum intensity of the hot state. The x and z coordinates are normalized to the operating wavelength $\lambda_0 = 4$ µm and the dashed black line marks the designed focal length of $20\lambda_0$. One can observe a clear focal spot in the hot state at $z \approx 24\lambda_0$. On the other hand, the cold state has nearly zero field intensity across the entire x-z plane.

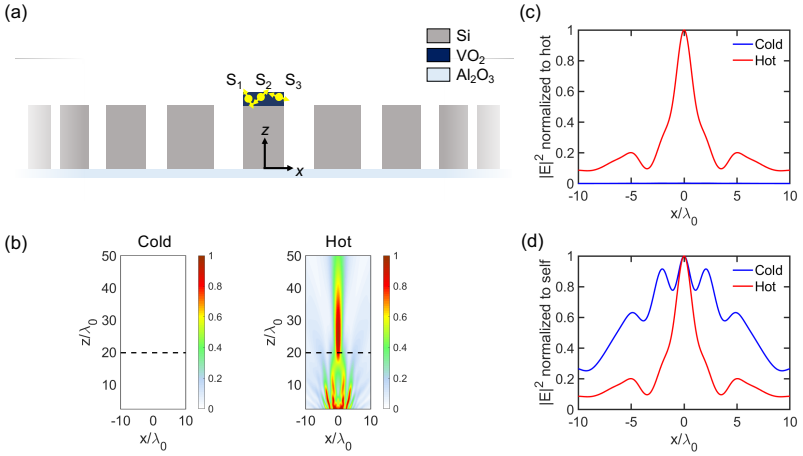

Fig. 4. (a) Schematic showing the dipole distribution for a calculation in which the dipoles are placed only in the VO_2 cap. (b) Field intensities in the x-z plane at a wavelength of 4 µm for the cold and hot states of a lens simulated with 600 dipoles. The intensities in both states are normalized to the maximum intensity of the hot state. (c) Focal plane intensities for the lens in both temperature states normalized to the focal plane intensity in the hot state at $x = 0$. (d) Focal plane intensities in the two temperature states normalized to their own intensity at $x = 0$.

Figure 4(c) shows the field intensity of the lens in the cold and hot states at the designed focal length of $20\lambda_0$. The field intensities in both temperature states are normalized to the maximum focal plane intensity in the hot state. The peak centered at $x = 0$ in the field intensity of the hot state represents the focal spot. The full width at half maximum (FWHM) of this peak is 9.2 µm, which is approximately 11% of the total width of the lens along the x direction (80 µm). Additionally, one can notice a sideband on either side of the central peak. The peak intensities of these sidebands are approximately 20% of the peak focal spot intensity.

In order to investigate the emission from the lens in the cold state, we plot the field intensities at the focal plane in the two temperature states normalized to their own maximum in Fig. 4(d). One can observe a central peak in the field intensity of the cold state flanked by two sidebands on either side. The peak intensities of these sidebands are more than 60% of the central peak intensity. In an actual measurement of the focal plane intensity in the cold state, one may not

Optics EXPRESS

be able to distinguish the focal spot from the background due to its poor intensity contrast with respect to the sidebands. On the other hand, the focal spot will be clearly visible in the hot state.

To understand the origin of the large emission sidebands in the cold state, we simulate the lens with a single dipole placed at the center of the VO_2 cap. Figure 5 presents the focal plane intensities of the lens in the two temperature states for different orientations of the dipole. The field intensities for both temperature states are normalized to the maximum intensity for a z-oriented dipole. It can be observed that the lens focuses in both states for a z-oriented dipole (solid lines in Figs. 5(a) and (b)). Figure 5(a) shows that in the cold state, both x- and y-oriented dipoles contribute a background intensity that is comparable to the central peak generated by the z-oriented dipole. On the other hand, in the hot state, the contributions from the x- and y-oriented dipoles are much smaller as compared to that from the z-oriented dipole (Fig. 5(b)).

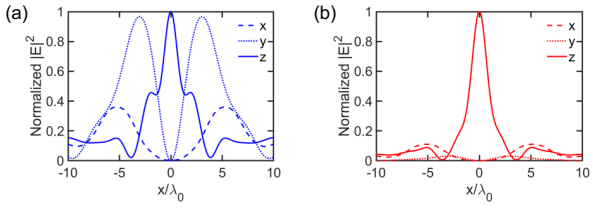

Fig. 5. Effect of dipole orientation on emission from the thermal lens. Focal plane intensity of the lens in the (a) cold and (b) hot states for different orientations of a single dipole placed at the center of the VO_2 cap.

In a typical thermal emission calculation for the lens in the cold state, dipoles not oriented along the z-axis will contribute a field intensity that is comparable to the focal spot. The contribution from such dipoles will be significantly smaller in the hot state resulting in a clear focal spot.

4. Discussion

It is important to note that the focal plane intensity of the lens is influenced by the operating temperature as well as the temperature-dependent permittivity of VO_2. In order to understand the relative contributions of these two factors to the overall emission from the lens, we examine two hypothetical situations.

We first consider a case in which the cap on the central resonator of the lens is made of a non-phase change material which has the same permittivity as metallic VO_2. Figure 6(a) presents the focal plane intensity of the lens at 300 and 350 K. The intensities are normalized to the maximum intensity of the lens at 350 K. One can notice that the intensity is larger in the hot state owing to its temperature. However, the lens focuses in both temperature states.

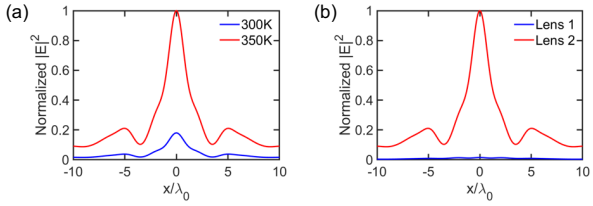

Fig. 6. (a) Focal plane intensities for a lens in which the cap on the central resonator is made of a non-phase change material which has the same permittivity as metallic VO_2. (b) Focal plane intensities for two lenses with the cap on the central resonator made of two different non-phase change materials. Lens 1 uses a material with a permittivity equal to that of insulating VO_2 while lens 2 uses one with permittivity equal to that of metallic VO_2.

Optics EXPRESS

Next, we consider two lenses with the cap on central resonator made of two different non-phase change materials. Lens 1 uses a material with a permittivity equal to that of insulating VO_2 while lens 2 uses one with permittivity equal to that of metallic VO_2. Figure 6(b) shows the focal plane intensities of the two lenses at a temperature of 300 K. The intensities are normalized to the maximum intensity of lens 2. One can notice a much larger difference in intensities of the two lenses as compared to Fig. 6(a). This is a result of the contrast in permittivities of the cap material of the two lenses. Additionally, while lens 2 has a clear focal spot, lens 1 has large emission sidebands (verified by looking at the intensity from lens 1 normalized to its own maximum). This follows from the analysis presented in Fig. 5.

We conclude from Fig. 6 that not only does the phase change of VO_2 result in a larger intensity contrast as compared to that obtained with only temperature difference, it also allows for selective thermal focusing in the hot state.

5. Conclusion

We proposed a microphotonic lens for achieving temperature-switchable self-focused thermal emission. By utilizing the coupling between isotropic Mie scatterers and the phase change properties of VO_2, we were able to design a lens to selectively emit focused radiation at a wavelength of 4 μm in the hot state. We validated the performance of our design by directly calculating thermal emission from the lens in both temperature states. For this purpose, we ran multiple, single-dipole FDTD simulations of the structure and added the results together incoherently with the appropriate scaling factors. Our calculations showed that not only does the lens have nearly zero intensity in the cold state relative to the hot state, it also has a smeared out focal spot in the cold state due to a large background emission. By examining two hypothetical scenarios, we deduced that the phase transition of VO_2 is crucial to achieving selective thermal focusing in the hot state.

Our switchable thermal lens could potentially benefit several applications. The ability to emit thermal radiation above a certain temperature at a desired wavelength could be useful for the construction of next-generation thermophotovoltaics. Microphotonic devices capable of emitting focused thermal radiation above a certain temperature could be used in conjunction with IR detectors for temperature monitoring and efficient contact-free sensing. One could also envision an on-chip infrared communication system in which such thermal lenses are utilized to establish a directional, free-space power flow between two predefined points. Given the wide range of applications, our switchable microphotonic lenses could pave the way for next-generation thermal sensing and infrared communication systems.

Funding. Defense Advanced Research Projects Agency (HR0011820046).

Acknowledgements. The authors would like to thank Virginia Wheeler and Vikrant Gokhale for helpful discussions.

Disclosures. The authors declare no conflicts of interest.

Data Availability. Data underlying the results presented in this paper are not publicly available at this time but may be obtained from the authors upon reasonable request.

References

1. J.-J. Greffet, R. Carminati, K. Joulain, J.-P. Mulet, S. Mainguy, and Y. Chen, "Coherent emission of light by thermal sources," Nature **416**(6876), 61–64 (2002).
2. R. Audhkhasi and M. L. Povinelli, "Spectral emissivity design using aluminum-based hybrid gratings," Opt. Express **28**(6), 8076–8084 (2020).
3. X. Liu, T. Starr, A. F. Starr, and W. J. Padilla, "Infrared Spatial and Frequency Selective Metamaterial with Near-Unity Absorbance," Phys. Rev. Lett. **104**(20), 207403 (2010).
4. X. Liu, T. Tyler, T. S. Starr, A. F. Starr, N. M. Jokerst, and W. J. Padilla, "Taming the Blackbody with Infrared Metamaterials as Selective Thermal Emitters," Phys. Rev. Lett. **107**(4), 045901 (2011).
5. S. Campione, F. Marquier, J.-P. Hugonin, A. R. Ellis, J. F. Klem, M. B. Sinclair, and T. S. Luk, "Directional and monochromatic thermal emitter from epsilon-near-zero conditions in semiconductor hyperbolic metamaterials," Sci. Rep. **6**(1), 34746 (2016).

Optics EXPRESS

6. I. Celanovic, D. Perreault, and J. Kassakian, "Resonant-cavity enhanced thermal emission," Phys. Rev. B **72**(7), 075127 (2005).
7. D. Constantini, A. Lefebvre, A.-L. Coutrot, I. Moldovan-Doyen, J.-P. Hugonin, S. Boutami, F. Marquier, H. Benisty, and J.-J. Greffet, "Plasmonic Metasurface for Directional and Frequency-Selective Thermal Emission," Phys. Rev. Applied **4**(1), 014023 (2015).
8. S. E. Han and C. J. Norris, "Beaming thermal emission from hot metallic bull's eyes," Opt. Express **18**(5), 4829–4837 (2010).
9. B. J. Lee, C. J. Fu, and Z. M. Zhang, "Coherent thermal emission from one-dimensional photonic crystals," Appl. Phys. Lett. **87**(7), 071904 (2005).
10. H. Zuo, D.-Y. Choi, X. Gai, P. Ma, L. Xu, D. N. Neshev, B. Zhang, and B. Luther-Davies, "High-Efficiency All-Dielectric Metalenses for Mid-Infrared Imaging," Adv. Opt. Mater. **5**(23), 1700585 (2017).
11. H. Chalabi, A. Alû, and M. L. Brongersma, "Focused thermal emission from a nanostructured SiC surface," Phys. Rev. B **94**(9), 094307 (2016).
12. M. Zhou, E. Khoram, D. Liu, B. Liu, S. Fan, M. L. Povinelli, and Z. Yu, "Self-Focussed Thermal Emission and Holography Realized by Mesoscopic Thermal Emitters," ACS Photonics **8**(2), 497–504 (2021).
13. W.-X. Huang, X.-G. Yin, C.-P. Huang, Q.-I. Wang, T.-F. Miao, and Y.-Y. Zhu, "Optical switching of a metamaterial by temperature controlling," Appl. Phys. Lett. **96**(26), 261908 (2010).
14. H. Wang, Y. Yang, and L. Wang, "Switchable wavelength-selective and diffuse metamaterial absorber/emitter with a phase transition spacer layer," Appl. Phys. Lett. **105**(7), 071907 (2014).
15. K. Ito, T. Watari, K. Nishikawa, H. Yoshimoto, and H. Iizuka, "Inverting the thermal radiative contrast of vanadium dioxide by metasurfaces based on localized gap-plasmons," APL Photonics **3**(8), 086101 (2018).
16. L. Lei, F. Lou, K. Tao, H. Huang, X. Cheng, and P. Xu, "Tunable and scalable broadband metamaterial absorber involving VO_2-based phase transition," Photonics Res. **7**(7), 734–741 (2019).
17. L. Long, S. Taylor, X. Ying, and L. Wang, "Thermally-switchable spectrally-selective infrared metamaterial absorber/emitter by tuning magnetic polariton with a phase-change VO_2 layer," Mater. Today Energy **13**, 214–220 (2019).
18. X. Song, Z. Liu, J. Scheuer, Y. Xiang, and K. Aydin, "Tunable polaritonic metasurface absorbers in mid-IR based on hexagonal boron nitride and vanadium dioxide layers," J. Phys. D: Appl. Phys. **52**(16), 164002 (2019).
19. R. Audhkhasi and M. L. Povinelli, "Design of far-field thermal rectifiers using gold-vanadium dioxide micro-gratings," J. Appl. Phys. (Melville, NY, U. S.) **126**(6), 063106 (2019).
20. L. Long, S. Taylor, and L. Wang, "Enhanced Infrared Emission by Thermally Switching the Excitation of Magnetic Polariton with Scalable Microstructured VO_2 Metasurfaces," ACS Photonics **7**(8), 2219–2227 (2020).
21. R. Audhkhasi and M. L. Povinelli, "Vanadium-dioxide microstructures with designable temperature-dependent thermal emission," Opt. Lett. **46**(7), 1768–1771 (2021).
22. J. B. Kana Kana, J. M. Ndjaka, G. Vignaud, A. Gibaud, and M. Maaza, "Thermally tunable optical constants of vanadium dioxide thin films measured by spectroscopic ellipsometry," Opt. Commun. **284**(3), 807–812 (2011).
23. A. Leitis, M. L. Tseng, A. John-Herpin, Y. S. Kivshar, and H. Altug, "Wafer-Scale Functional Metasurfaces for Mid-infrared Photonics and Biosensing," Adv. Mater. (Weinheim, Ger.) **33**, 2102232 (2021).
24. R. El-Ganainy and J. Sajeev, "Resonant dipole-dipole interaction in confined and strong-coupling dielectric geometries," New J. Phys. **15**(8), 083033 (2013).
25. Z. Ruan and S. Fan, "Temporal coupled-mode theory for light scattering by an arbitrarily shaped object supporting a single resonance," Phys. Rev. A **85**(4), 043828 (2012).
26. D. L. C. Chan, M. Soljacic, and J. D. Joannopoulos, "Direct calculation of thermal emission for three-dimensionally periodic photonic crystal slabs," Phys. Rev. E **74**(3), 036615 (2006).
27. S. E. Han and D. J. Norris, "Control of Thermal Emission by Selective Heating of Periodic Structures," Phys. Rev. Lett. **104**(4), 043901 (2010).